Lasers in Manufacturing Conference 2017

Comprehensive analysis of selective laser melting of TiAl powder

M. Doubenskaia[a], A. Domashenkov[a], I. Smurov[a,*], P. Petrovskiy [b]

[a]*Lyon University, ENISE, LTDS Laboratory, UMR CNRS 5513, 58 rue Jean Parot, 42023 Saint-Étienne Cedex 2, France*
[b]*Nation University of Science & Technology (MISIS), 4 Leninsky pr., 119049, Moscow, Russia*

Abstract

Selective laser melting of intermetallic Ti–48Al–2Cr–2Nb powder is studied using parametric analysis, metallography, optical diagnostics and mathematical modeling. Two substrate materials are compared: Steel S235 and pure Al. Preheating up to 450 °C is applied for manufacturing of cubic samples. Resulting porosity versus processing parameters is analyzed.
The average microhardness of the manufactured samples varies in the range of 540-559 $HV_{0.3}$.
XRD analysis shows prevailing of the α_2-Ti_3Al phase in the initial powder, heat treated powder and developed samples. Some minor peaks of γ-TiAl appeared in SLM processed specimens. EDS analysis shows the effect of Al evaporation, which intensifies with laser input energy.
The IR-camera is used for optical diagnostics of a single track formation. The geometry of heat affected zone versus processing parameters is analyzed. The evaporation of Al is detected by IR-camera for the elevated laser energy.
Mathematical modeling reveals that the same region of a sample can be remelted several times during fabrication, depending on the SLM processing parameters and strategy of beam scanning. The maximum calculated cooling rates are of the order of 10^6 °C/sec.

Keywords: Selective Laser Melting, intermetallics, optical diagnostics, Al evaporation, thermo-cycling.

* Corresponding author. Tel.: +33 4 77 43 75 61.
E-mail address: igor.smurov@enise.fr

1. Introduction

The remarkable properties of titanium aluminides, such as ratio of strength to density, thermodynamic stability, high temperature strength and oxidation resistance, coupled with low specific weight (~ 4 g/cm^3) compared to super alloys (~ 8.5 g/cm^3) create favorable perspectives for their application in aerospace, biomedical, energy engineering applications, etc. (Hood, 2010; Imayev, Imayev, Oehring, & Appel, 2007; Leyens & Peters, 2006).

The traditional methods of titanium aluminide synthesis, based on furnace metallurgy, have a number of disadvantages due to the high chemical reactivity of basic components at elevated temperatures, large difference in densities, melting and boiling points of initial components, that requires to apply vacuum equipment, like vacuum plasma-arc, electron beam remelting, etc.

Selective Laser Melting (SLM) is one of the AM methods, when a component is manufactured layer-by-layer by fusing of a powder bed by a laser beam. Particular features of the physical phenomena involved in SLM are related to strong modifications of heat and radiation transfer (Gusarov & Kruth, 2005) during powder melting by the laser beam.

2. Methods

Selective laser melting of the Ti–48Al–2Cr–2Nb powder is carried out using an SLM machine Phenix Systems «PM-100», equipped with a continuous fiber laser of 1073 nm wavelength (IPG Photonics Corp.), 200 W maximum power with spot diameter of 70 μm.

Steel S235 and pure Al are used as building-substrate materials. The building chamber was protected by argon.

The powder size distribution is studied using a granulomorphometer ALPAGA 500NANO (OCCHIO S.A.).

Scanning Electron Microscopy (SEM) images of the powder and samples are obtained by an electron microscope S-3400N (Hitachi High-Technologies Corporation), equipped with a NORAN energy-dispersive X-ray spectrometer.

The samples for metallographic analysis are prepared on Phoenix 4000 (BUEHLER, USA) grinder polisher. Optical micrography is performed with ZEISS Axioscope A1 optical microscope. X-ray diffraction (XRD) measurements for the samples are obtained on DRON-4 automatic diffractometer using monochromatic CuKα radiation in step-by-step scanning mode in the 2θ range of 10-110° with the scan increment of 0.1°

The microhardness tests are performed with BUEHLER Micromet 5104, using a load of 300 g for all tests. The indention duration was 15 sec.

Optical diagnostics of single tracks was carried out using laboratory set-up including an IR-camera and a closed box with protective gas atmosphere (Ar) where the substrate, covered by a powder layer of 30 μm, was placed.

The IR-camera (FLIR Phoenix RDAS^{TM}) with an InSb sensor and 3 – 5 μm bandpass arranged on 320 × 256 pixels array, with a frame rate of up to 38 kHz, when using sub-windows, was installed at the 45° angle to the zone of fabrication. A zone of IR-camera vision is 4.5x7 mm^2.

The optical diagnostics was performed using a fiber laser IPG Photonics Corp., 200 W maximum power, laser spot diameter equals to 150 μm and a scanner-head HurryScan 14 by SCANLAB, Germany with an effective focal distance of 420 mm and a maximum beam scanning velocity up-to 7 m/s.

Powder layering was carried out with the help of an industrial SLM machine Phenix Systems «PM-100» that is capable to deposit regular powder layers up-to 20 μm thickness. Then the substrate, covered by the powder, was transferred into an isolated optical diagnostic set-up. The titanium alloy Ti-6Al-4V was used as a substrate material in optical diagnostics experiments.

Surface profiles of single tracks were examined by an optical profilometer “WYKO NT 1100”.
The software PTC Mathcad 15.0 is used for mathematical modelling.

3. Materials

The intermetallic Ti–48Al–2Cr–2Nb powder has been provided by TLS Technik GmbH. According to the SEM, powder particles have generally a spherical form (Fig. a). The average diameter of the particles is equal to 30 µm (Fig. b).

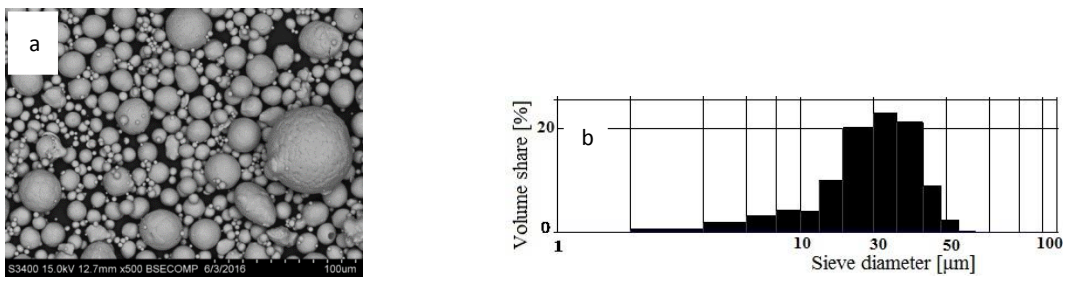

Fig. 1. (a) SEM image of the Ti–48Al–2Cr–2Nb powder (b) particle size distribution

The chemical composition of the utilized powder according to the Energy-dispersive X-ray spectroscopy (EDS) is presented in Table 1.

Table 1. Chemical composition of the initial powder by EDS

Element	Al	Ti	Nb	Cr
wt.%	31.57	61.98	2.45	4.00
at.%	45.48	50.86	1.86	1.78

4. Results and discussion

4.1. SLM process

Two substrates have been applied in experiments with single tracks formation: steel S235 and pure Al. The experiments were carried out in the following range of parameters: laser power 50-150 W, beam scanning velocity 100–1500 mm/sec; powder layer thickness 60 µm. The general tendency is the enlargement of optimum parametric windows passing from 50 to 100 W. With further increase of power up to 150 W, the shape of the tracks becomes irregular because of excess of a liquid phase. The increase of the scanning velocity results in narrowing of the SLM track.

The results reveal the insufficient metallurgical contact for the steel substrate that is why it has been excluded from further experiments.

The SLM parametric analysis (Mertens et al., 2014; Yadroitsev, Bertrand, & Smurov, 2007) of the Ti–48Al–2Cr–2Nb powder has shown that the optimal single track geometry was achieved for the laser power of P=90 W.

The cubic samples of 7x7x7 mm^3 volume have been fabricated. The crosswise strategy is applied, when the laser scan direction turns by 90° after each layer deposition cycle.

For the processing of 3D samples, it was proposed to apply *in-situ* heating in order to decrease possible residual stresses by reducing thermal gradients. The complete volume of the fabrication chamber has been preheated up to 450 °C by the integrated furnace. The argon filling started with the pre-heating cycle, 2 hours before the SLM process.

The resulting density is measured by the image contrast method (Table 2). The cracks are counted during measurements. The variation of density value is related to the contrast adjustment of the cross-section images.

Table 2. Effect of the scanning speed on the effective linear energy input and density of samples obtained on Al substrate

Laser power, W	Layer thickness, µm	Hatch distance, µm	Beam scanning speed, mm/s	Effective linear energy input, J/mm	Density, %
90	60	90	600	0.15	92.7±2.2
		90	800	0.11	77.2±1.8
		80	1000	0.09	84.3±2.4
		80	1400	0.06	78.3±2.1

Intermetallic alloys are known as compounds with elevated brittleness. Loeber et al. (Loeber et al., 2011) has reported the crack formation in specimens from Ti-48Al-2Cr-2Nb obtained by SLM.

The large size of the molten pool at low scanning speed, 600 mm/s, leads to decreasing the quantity of small pores, which appear probably due to Al boiling. The large pores with the size of tens and even hundreds of microns were found in interlayer and intertrack regions.

4.2. Phase composition and microstructure

According to the phase diagram of the Ti-Al system (Fig.), there are four stable intermetallic phases: Ti_3Al, γ-TiAl, $TiAl_3$ and $TiAl_2$ (Rocha, Ariza, Costa, Oliveira, & Silva, 2003). Ti_3Al compound, also known as α_2-phase, has the long-range ordered hexagonal $D0_{19}$ (*hP8*) structure (Banumathy, Ghosal, & Singh, 2005).

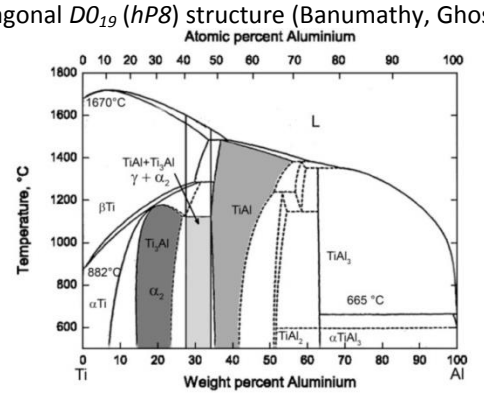

Fig. 2. Ti–Al phase diagram

Ti_3Al-base alloys have elevated tensile and yield strength properties but also high brittleness at normal temperatures, comparing to γ-TiAl-based materials. The titanium aluminide γ-TiAl has tetragonal $L1_0$ (*CuAl*-type) structure. This phase has better resistance to creep and oxidation at high temperatures (up to 900-1000 °C) (Sauthoff, 2008).

Increasing of Al content results in formation of titanium di- and tri-aluminides. Both phases lead to increasing of hardness and brittleness of the material (Rastkar, Parseh, Darvishnia, & Hadavi, 2013). There

are two known closely related modifications of $TiAl_2$ lattice structure: tetragonal *$HfGa_2$*-type and orthorhombic *$ZrGa_2$*-type. The $TiAl_3$ phase could have one of the two structure modifications: cubic *$L1_2$* or tetragonal *DO_{22}* (Sauthoff, 2008).

The results of the XRD analysis show prevailing of the Ti_3Al phase in both powder and obtained samples. No significant difference in phase composition between the initial and the heat-treated powders was detected (Fig. a). Some minor peaks of γ-TiAl appear in the manufactured specimens comparing to the powder (Fig. a vs b). Moreover, the difference between the samples, processed with scanning speeds of 600 and 1400 mm/s is almost negligible.

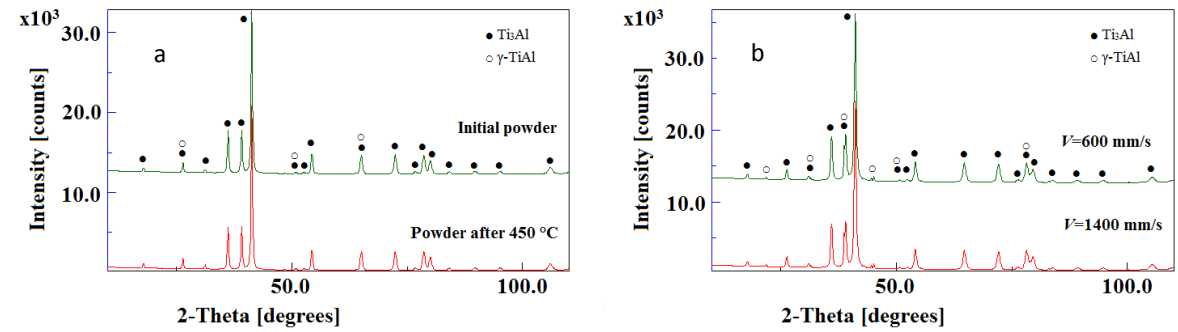

Fig. 3. X-ray patterns (a) initial and heat-treated powder (b) manufactured samples

Kothari et al. (Kothari, Radhakrishnan, & Wereley, 2012) report the following main types of the α_2 phase microstructure, depending on the manufacturing technique and post heat treatment: bi-modal, equiaxed and lamellar.

Bi-modal structure shows enhanced ductility at normal temperature but quite low creep resistance at temperatures over 600 °C.

Non-uniform composition of the SLM processed samples is related to the difference in vapor pressure of Ti and Al at the same temperature. The melting point of Al is 933 K and that of Ti is 1943 K, the boiling points are 2793 and 3562 K, respectively. At the melting point of Ti, the vapor pressure of pure Al is about $3.6 \cdot 10^{-2}$ Pa. Experimental results presented in (Maeda, Kiwake, Shibuya, & Ikeda, 1997) have shown substantial Al loss with almost negligible Ti losses during holding of TiAl at constant temperature in electron beam vacuum furnace.

In addition, non-uniformity of the composition is attributed to the high reactivity and solubility of oxygen, nitrogen and other gaseous elements in liquid phase of Ti. During SLM of Ti and Ti-base alloys, the molten pool can be easily contaminated by even minor impurities from the ambient atmosphere. Because of this problem the remelting or fabrication of intermetallic feedstock material is usually conducted under vacuum conditions. Even small amount of absorbed oxygen or nitrogen dramatically reduce the ductility of TiAl materials. That is why in SLM of TiAl the efficient application of protection atmosphere is extremely important.

4.3. Optical diagnostics

The optical diagnostic is applied in order to study the Al evaporation effects. The images of the IR-camera for different beam scanning velocities are compared with photos of the corresponding tracks (Fig. 4). The general tendency is narrowing of the track width and decreasing of the size of zone of highest thermal signal with beam scanning velocity. In addition, general elongation of the thermal signal recorded by the IR-

camera, with beam scanning velocity is found. The “fish tail” geometry of the right side of the thermal radiation field, in particular for Fig. b, c is related to the significant difference of thermal conductivities (order of 20 times, according to (Gusarov, Yadroitsev, Bertrand, & Smurov, 2009)) between the un-melted powder and the powder, consolidated into a track. The heat flux is oriented mainly in the direction from the molten pool towards the solidified track.

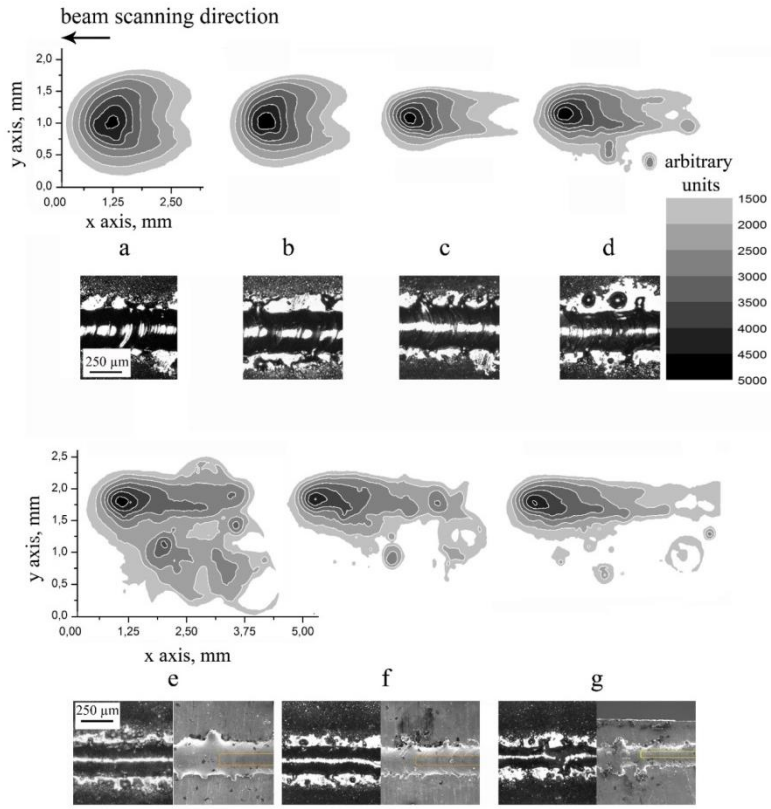

Fig. 4. IR-camera images of thermal emission field during SLM of Ti-48Al-2Cr-2Nb powder and tracks top view (optical microscope for all images, plus SEM images for figures (e-g)), P=50 W, (a) V=1 mm/s (b) V=5 mm/s (c) V=10 mm/s (d) V=20 mm/s (e) V=50 mm/s (f) V=100 mm/s (g) V=200 mm/s.

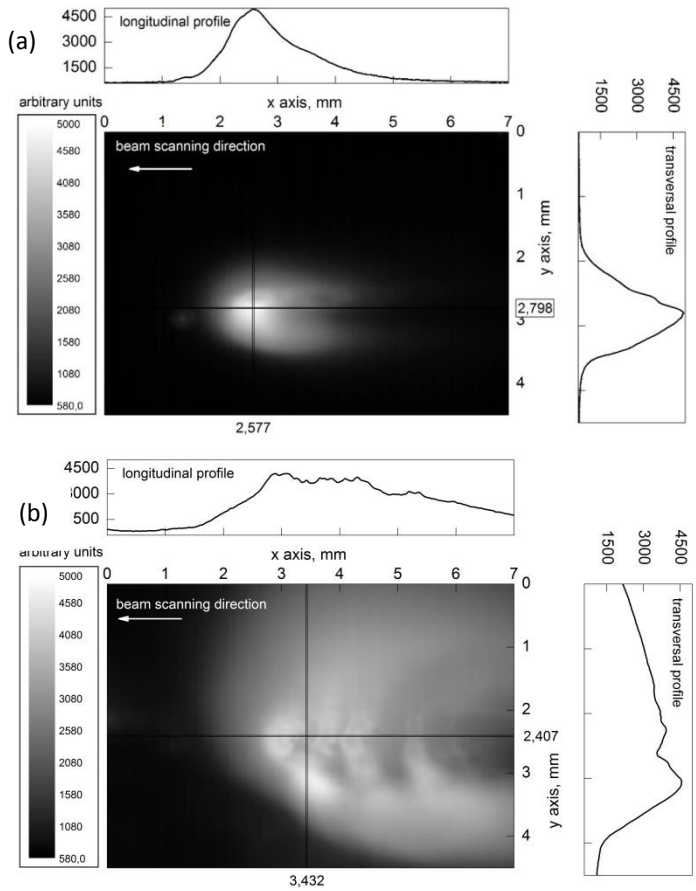

Fig. 5. IR-camera images of intensity of thermal radiance and its profiles during SLM of Ti-48Al-2Cr-2Nb powder, V=5 mm/s (a) P=50 W (b) P=150 W

The intensification of hydrodynamic instabilities and material rejection from the zone of powder consolidation with beam scanning velocity is found (Fig. e, f, g). The shape of corresponding tracks becomes irregular. With the further velocity increase, the continuous track is decomposed on individual droplets because of Plateau–Rayleigh instability (Gusarov, Yadroitsev, Bertrand, & Smurov, 2007).

The IR-camera images of the thermal emission field and the corresponding profiles are rather different in Fig. a, b: the narrow transversal profile and the shorter longitudinal one for 50 W laser power (Fig. a) and, on the contrary, the thermal emission field for 150 W is strongly perturbed by Al vapor (Fig. b).

4.4. Al losses

In (Gussone et al., 2015) the influence of the laser power on segregation and losses of Al was studied. Authors supposed that Al segregation takes place at the bottom of the molten pool, while the regions of Al losses are located close to its surface where the temperature is maximum. According to the EDS profiles, measured at the center of single tracks' cross-sections (Fig. b,e), from top to bottom, this tendency is not

confirmed (Fig. c vs f). For certain processing windows the near-surface concentration of Al is higher than the one inside of the track. This effect could be related to the thermo-capillary convection.

The thermo-capillary effects can be associated with the so-called zone of dissolution. To measure the dissolution zone, the tracks were analyzed by an optical profilometer (Fig. b, e). The dissolution zone depth is determined as the distance between the initial top surface of the substrate and the zone with constant composition of Ti and Al inside the substrate (Fig. c, f). According to the obtained data, the dissolution depth increases with laser input energy.

Defects of the samples look far different in two cases: (a) for insufficient energy input incomplete powder melting results in formation of large pores in certain regions; (b) while high energy input initiates cracking. Both high power and high scanning velocity lead to increased productivity, less stress and oxygen content.

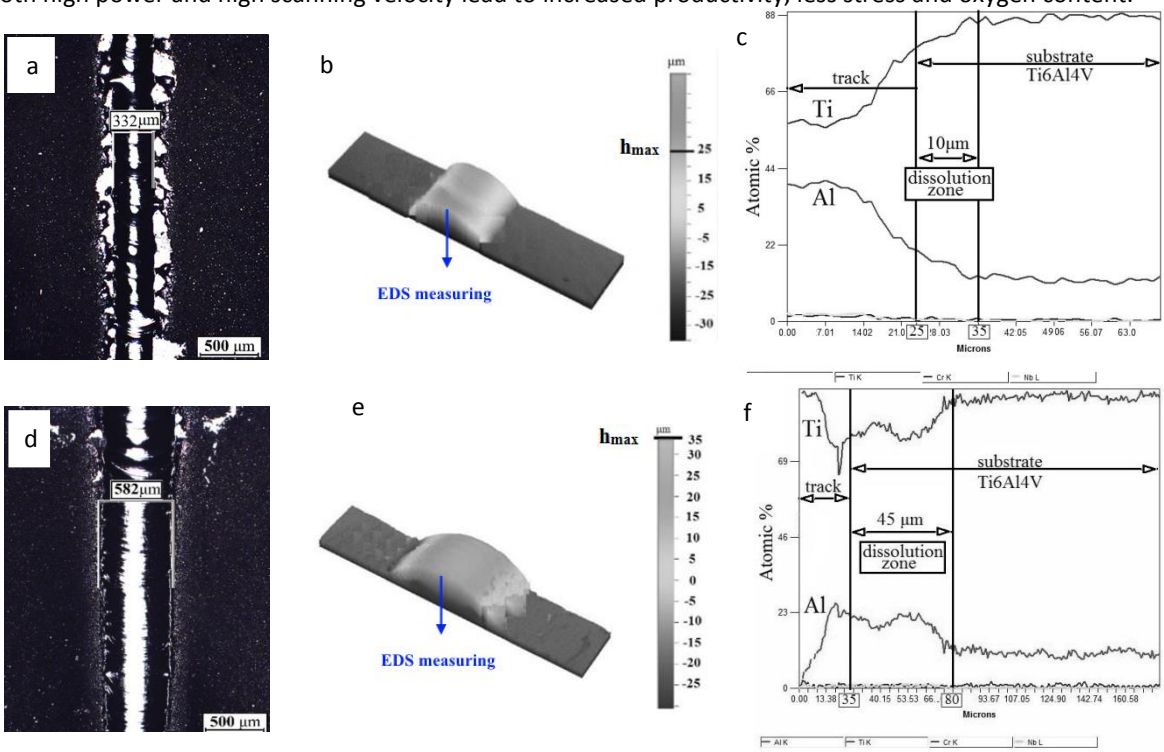

Fig. 6. Optical micrography, 3D images and EDS distribution of Ti and Al within the depth of the manufactured track at (a, b, c) *V*=5 mm/s, *P*=50 W, *h*=30 µm, (d, e, f) *V*=5 mm/s, *P*=150 W, *h*=30 µm.

4.5. Mathematical modeling

A self-consistent model of SLM is far from complete development. This is because of a large number of involved physical phenomena including laser radiation transfer, melting/solidification, evaporation, melt hydrodynamics and many others.

Important problematic is related to the analysis of thermal cycles in a fixed point, during manufacturing of an SLM part. A model, providing information on temperature evolution and heating/cooling rates, is useful to estimate the influence of processing parameters on the resulting microstructure. Evidently, the development of a complicated model, taking into account radiation transfer and phase transitions, as for

example in (Gusarov & Smurov, 2010), is far outside of the domain of commercially available simulation software, suitable for SLM process modeling.

The simplified heat transfer model, based on the analytical solutions developed by N. Rykalin (Rykalin, 1951, 1960) was used for estimation of the eventual superposition of temperature fields resulting from individual laser scanning tracks (Domashenkov, 2013; Kotoban, 2013). The analytical solution corresponding to the Gaussian heat source, moving on the surface of semi-infinite body has been selected as a basic element of the model. At the next step, the superposition principle is applied to summarize temperature fields from different heating sources, which is valid for linear heat transfer models. The distance between the individual passages of the heat source corresponds to the hatch distance.

Table 3. Thermo-physical properties of Ti–48Al–2Cr–2Nb

Properties, at 600 °C	Designation	Value
Density, kg/cm^3 (Egry et al., 2007)	ρ	0.0041
Thermal capacity, J/(kg·K) (Zhang, Reddy, & Deevi, 2001)	c	700
Thermal conductivity, W/(cm·K) (Zhang et al., 2001)	λ	0.23
Thermal diffusivity, cm^2/s (Egry et al., 2007)	a	0.08
Absorptivity, %	A	90
Melting point, °C (Saari, Seo, Blumm, & Beddoes, 2003)	T_M	1460

Only heat conduction in solid state is considered, that is why the temperature curves are limited by the melting point of the powder material. The ambient temperature used in modelling is 450 °C, which corresponds to the experimental conditions. The applied thermo-physical parameters of Ti–48Al–2Cr–2Nb are taken at T=600 °C (Table).

The temperature profile after 3 passages of the heat source, separated by a hatch distance, are calculated at the surface of the powder layer, in a fixed point, located at the center of the 2nd passage (Fig.). For V=600 mm/s and S=90 µm, melting takes place for all three laser passes, which indicates relatively large molten pool size. When V=1400 mm/s and S=80 µm, laser beam melts only once when passing through the selected point.

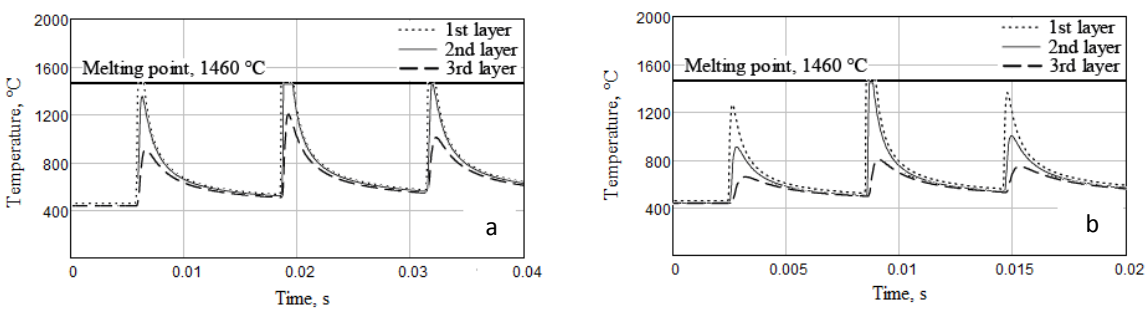

Fig. 7. Simulation of thermal cycles for SLM processing of Ti–48Al–2Cr–2Nb cubic samples, P=90 W, h=60 µm, T=450 °C (a) V=600 mm/s, S=90 µm (b) V=1400 mm/s, S=80 µm.

5. Conclusions

All the specimens were manufactured on Al substrate and are characterized by a number of cracks. Moderate scanning speeds lead to decreasing of the resulting porosity but the increased thermal impact stimulate crack propagation. The density of 93 ± 2 % was obtained for the following process parameters: laser power - 90 W, beam scanning speed - 600 mm/s, powder layer thickness - 60 µm, hatch distance - 90 µm, preheating temperature - 450 °C.

The main difficulty in laser processing of TiAl is related to the considerable difference of Ti and Al thermal and physical properties, in particular to different melting and boiling points.

The average microhardness of the manufactured samples varies in the range of 540-559 $HV_{0.3}$. The microhardness variation confirmed the anisotropy of all the fabricated samples. The insufficiency of the 450 °C preheating temperature for eliminating of the inhomogeneity was shown.

The XRD analysis revealed prevailing of the brittle α_2-Ti_3Al phase in the initial powder, manufactured specimens and in the preheated up to 450 °C powder. The pronounced lamellar microstructure was observed in all samples after SLM. This type of structure leads to the elevated brittleness of the α_2-Ti_3Al phase, which finally determines crack formation and propagation.

The EDS analysis confirmed the intensification of the Al evaporation with laser input. The fraction of Al has decreased from initial 45.8%at. to 44.8%at. and to 43.9%at. for the samples, processed with the scanning speeds of 1400 mm/s and 600 mm/s, respectively. The near-surface concentration of Al is defined by the applied laser energy.

Optical diagnostic was applied to define the regularities of heat - and mass transfer in SLM. According to the IR-camera, the elongation of HAZ with beam scanning velocity was detected. The “fish tail” geometry of the thermal radiation field behind the laser action zone is related to the significant difference of thermal conductivities between the unmelted powder and the powder consolidated into a track. Intensity of Al evaporation versus SLM parameters was detected.

Mathematical modeling shows that depending on the SLM processing parameters and strategy of beam scanning, the same region of a sample can be remelted several times during fabrication. The cooling rates in solid state, with maximum values of the order of 10^6 °C/sec, were found.

Acknowledgment

The work was carried out with financial support from the Ministry of Education and Science of the Russian Federation in the framework of Increase Competitiveness Program of NUST «MISiS» (№ К1-2016-030), implemented by the governmental decree dated on 16th of March 2013, N 211.

References

Banumathy, S., Ghosal, P., & Singh, A. (2005). On the structure of the Ti 3 Al phase in Ti–Al and Ti–Al–Nb alloys. *Journal of alloys and compounds, 394*(1), 181-185.

Domashenkov, A. (2013). *Fabrication des moules pour moulage par injection au moyen de la fusion sélective par laser.* (Diplôme de Master Recherche), l'Université de Lyon.

Egry, I., Brooks, R., Holland-Moritz, D., Novakovic, R., Matsushita, T., Ricci, E., . . . Jarvis, D. (2007). Thermophysical properties of γ-titanium aluminide: the European IMPRESS project. *International journal of thermophysics, 28*(3), 1026-1036.

Gusarov, A., & Kruth, J.-P. (2005). Modelling of radiation transfer in metallic powders at laser treatment. *International Journal of Heat and Mass Transfer, 48*(16), 3423-3434.

Gusarov, A., & Smurov, I. (2010). Radiation transfer in metallic powder beds used in laser processing. *Journal of Quantitative Spectroscopy and Radiative Transfer, 111*(17), 2517-2527.

Gusarov, A., Yadroitsev, I., Bertrand, P., & Smurov, I. (2007). Heat transfer modelling and stability analysis of selective laser melting. *Applied surface science, 254*(4), 975-979.

Gusarov, A., Yadroitsev, I., Bertrand, P., & Smurov, I. (2009). Model of radiation and heat transfer in laser-powder interaction zone at selective laser melting. *Journal of heat transfer, 131*(7), 072101.

Gussone, J., Hagedorn, Y.-C., Gherekhloo, H., Kasperovich, G., Merzouk, T., & Hausmann, J. (2015). Microstructure of γ-titanium aluminide processed by selected laser melting at elevated temperatures. *Intermetallics, 66*, 133-140.

Hood, R. (2010). *The Machinability of a Gamma Titanium Aluminide Intermetallic.* (Ph.D. thesis), University of Birmingham. Retrieved from https://books.google.fr/books?id=hh6lngEACAAJ

Imayev, R., Imayev, V., Oehring, M., & Appel, F. (2007). Alloy design concepts for refined gamma titanium aluminide based alloys. *Intermetallics, 15*(4), 451-460.

Kothari, K., Radhakrishnan, R., & Wereley, N. M. (2012). Advances in gamma titanium aluminides and their manufacturing techniques. *Progress in Aerospace Sciences, 55*, 1-16.

Kotoban, D. (2013). *Étude de dépôt des revêtements fonctionnels multimatériaux par rechargement laser pour diverses applications tribologiques.* (Diplôme de Master Recherche), l'Université de Lyon.

Leyens, C., & Peters, M. (Eds.). (2006). *Titanium and Titanium Alloys: Fundamentals and Applications*. Cologne, Germany: John Wiley & Sons.

Loeber, L., Biamino, S., Ackelid, U., Sabbadini, S., Epicoco, P., Fino, P., & Eckert, J. (2011). *Comparison of selective laser and electron beam melted titanium aluminides.* Paper presented at the Proceedings of the Solid Freeform Fabrication Symposium, Austin, TX, USA.

Maeda, M., Kiwake, T., Shibuya, K., & Ikeda, T. (1997). Activity of aluminum in molten Ti–Al alloys. *Materials Science and Engineering: A, 239*, 276-280.

Mertens, A., Reginster, S., Paydas, H., Contrepois, Q., Dormal, T., Lemaire, O., & Lecomte-Beckers, J. (2014). Mechanical properties of alloy Ti–6Al–4V and of stainless steel 316L processed by selective laser melting: influence of out-of-equilibrium microstructures. *Powder Metallurgy, 57*(3), 184-189.

Rastkar, A. R., Parseh, P., Darvishnia, N., & Hadavi, S. M. M. (2013). Microstructural evolution and hardness of TiAl 3 and TiAl 2 phases on Ti–45Al–2Nb–2Mn–1B by plasma pack aluminizing. *Applied surface science, 276*, 112-119.

Rocha, L. A., Ariza, E., Costa, A. M., Oliveira, F. J., & Silva, R. F. (2003). Electrochemical behavior of Ti/Al2O3 interfaces produced by diffusion bonding. *Materials Research, 6*(4), 439-444.

Rykalin, N. (1951). *Расчеты тепловых процессов при сварке (Calculation of heat processes in welding) (In Russian)*. Moscow: Mashgiz.

Rykalin, N. (1960). *Calculation of heat processes in welding*. Paper presented at the 42nd annual meeting of american welding society, New York.

Saari, H., Seo, D., Blumm, J., & Beddoes, J. (2003). Thermophysical property determination of high temperature alloys by thermal analysis. *Journal of Thermal Analysis and Calorimetry, 73*(1), 381-388.

Sauthoff, G. (2008). *Intermetallics*. Würzburg, Germany: Wiley.

Wohlers, T. (2014). Wohlers Report 2014: 3D Printing and Additive Manufacturing State of the Industry; Wohlers Associates. *Inc.: Fort Collins, CO, USA*.

Yadroitsev, I., Bertrand, P., & Smurov, I. (2007). Parametric analysis of the selective laser melting process. *Applied surface science, 253*(19), 8064-8069.

Zhang, W., Reddy, B., & Deevi, S. (2001). Physical properties of TiAl-base alloys. *Scripta Materialia, 45*(6), 645-651.